

Surgical Gaussian Surfels: Highly Accurate Real-time Surgical Scene Rendering

Idris O. Sunmola¹, Zhenjun Zhao², Samuel Schmidgall¹, Yumeng Wang¹, Paul Maria Scheikl¹, and Axel Krieger¹

¹Johns Hopkins University, Baltimore, MD, USA

²Chinese University of Hong Kong (CUHK), Hong Kong, China

{isunmola1} @ jhu.edu

Abstract. Accurate geometric reconstruction of deformable tissues in monocular endoscopic video remains a fundamental challenge in robot-assisted minimally invasive surgery. Although recent volumetric and point primitive methods based on neural radiance fields (NeRF) and 3D Gaussian primitives have efficiently rendered surgical scenes, they still struggle with handling artifact-free tool occlusions and preserving fine anatomical details. These limitations stem from unrestricted Gaussian scaling and insufficient surface alignment constraints during reconstruction. To address these issues, we introduce Surgical Gaussian Surfels (SGS), which transforms anisotropic point primitives into surface-aligned elliptical splats by constraining the scale component of the Gaussian covariance matrix along the view-aligned axis. We predict accurate surfel motion fields using a lightweight Multi-Layer Perceptron (MLP) coupled with locality constraints to handle complex tissue deformations. We use homodirectional view-space positional gradients to capture fine image details by splitting Gaussian Surfels in over-reconstructed regions. In addition, we define surface normals as the direction of the steepest density change within each Gaussian surfel primitive, enabling accurate normal estimation without requiring monocular normal priors. We evaluate our method on two in-vivo surgical datasets, where it outperforms current state-of-the-art methods in surface geometry, normal map quality, and rendering efficiency, while remaining competitive in real-time rendering performance. We make our code available at <https://github.com/alomaa85/SurgicalGaussianSurfels>

Keywords: Gaussian Splatting · 3D Surface Reconstruction · Minimally Invasive Surgery.

1 Introduction

Reconstructing dynamic surgical scenes from endoscopic videos is a crucial, yet complex task in robot-aided minimally invasive surgery. Accurate reconstructions improve the precision of surgical instrument manipulation and serve as a foundation for clinical applications such as AR/VR surgical simulation, medical training, and complete medical automation [2]. Factors such as deformable

tissues, limited viewing angles, surgical tool occlusion, and severe specularity currently thwart existing 3D surface rendering methods [4].

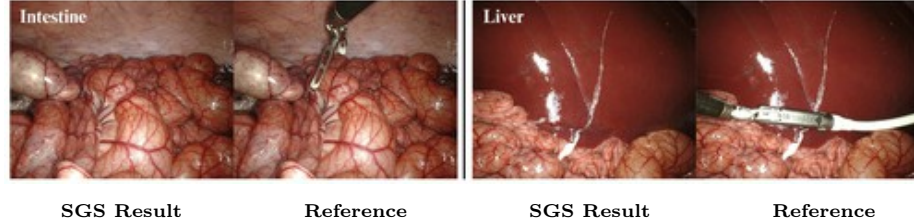


Fig. 1: Qualitative results of our method SGS on the StereoMIS [5] Intestine and Liver dataset. We remove surgical tools and render artifact-free surgical tissue.

Advancements in 3D Gaussian Splatting (3DGS) [8] have shown promise in rendering and reconstructing 3D surgical scenes efficiently. Despite these advancements, 3DGS struggles with accurate geometric reconstructions, primarily due to the non-zero thickness of Gaussian point primitives and the ambiguity in normal directions due to their ellipsoid-like shape [1]. To address these limitations, Gaussian Surfels have been proposed, which flatten 3D Gaussian points into 2D ellipses by setting the z-scale to zero [1].

In this paper, we introduce Surgical Gaussian Surfels (SGS), a novel method that combines the surface alignment properties of Gaussian Surfels with the dynamic modeling capabilities of Gaussian Splatting to reconstruct deformable tissues in endoscopic videos. Occluding surgical instruments introduce challenges in reconstruction by obstructing the view of underlying tissues and introducing motion-appearance ambiguities in single-viewpoint scenarios. We address this by incorporating depth priors and a binary motion mask during Gaussian Surfel initialization and training, effectively filtering out occluding instruments and improving reconstruction accuracy.

Our **contributions** are as follows: (1) We propose SGS, a point-primitive-based rendering technique that takes advantage of the surface-alignment benefits and the high-quality rendering abilities of Gaussian Surfels to achieve high-fidelity reconstruction of dynamic surgical scenes; (2) By defining surface normals as the direction of the steepest density change within each surfel primitive, we accurately predict the orientation of surgical tissue without relying on monocular normal priors, thereby enhancing reconstruction geometry and mitigating shape-radiance ambiguities in highly specular areas; (3) We introduce a Projection-Based Iterative Mask Integration (PIMI) method to initialize point clouds in surgical scenes, resolving gaps and inaccuracies caused by incomplete depth data through confidence-weighted depth aggregation and refined color mapping; (4) SGS outperforms prior implicit and explicit rendering techniques in both quantitative and qualitative experiments.

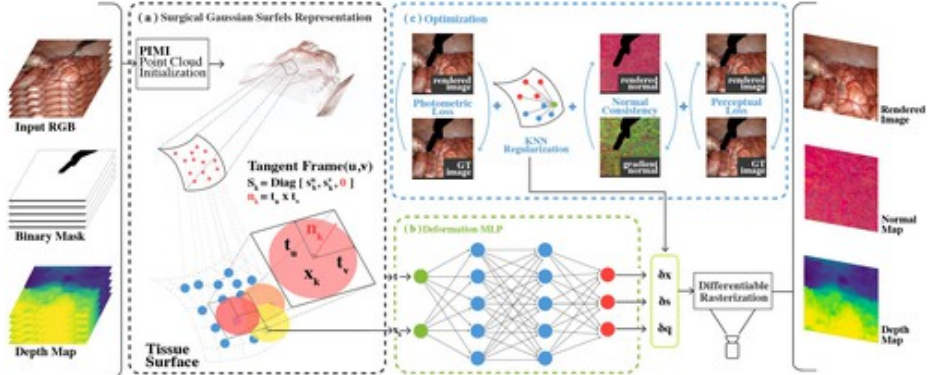


Fig. 2: **Method pipeline.** The full video sequence frames, Binary Mask, Depth Map is passed through PIMI; (a) 2D points are projected to 3D then the tissue surface is represented as Gaussian Surfels with scaling matrix S_k , tangent vectors t_u and t_v , and position x_k ; (b) Deformation prediction MLP takes Surfel position x_k and normalized timestamp t then predicts the change in position δx , scale δs , and rotation δq ; (c) Optimization of Surgical Gaussian Surfels. Pipeline outputs an occlusion-free rendered surgical scene, normal map, and depth map.

2 Related Work

Recent advances in endoscopic 3D reconstruction have been driven by neural-radiance fields and explicit representations. EndoNerf [16] introduces a dual network architecture that combines implicit neural fields with mask-guided ray casting for tool occlusion and depth-cueing ray marching for single-viewpoint reconstruction. EndoSurf [20] advances this framework by representing the canonical scene using signed distance functions (SDF). Neural LerPlane [18] decomposes 4D surgical scenes by factorization into explicit 2D planes of static and dynamic fields to address the computational overhead of volumetric neural fields. EndoGaussian [10] marks a shift towards explicit representations by introducing Holistic Gaussian Initialization (HGI). Endo-4DGS [7] leverages the Depth-Anything foundation model for robust initialization and implements confidence-guided learning to handle uncertain depth measurements in deformable tissues. SurgicalGaussian [17] addresses the limitation of planar structures in encoding complex motion fields by using a deformation network that decouples motion and geometry. Our method builds on and surpasses these prior methods in artifact-free surgical tool removal and tissue reconstruction.

3 Method

Our pipeline, shown in Fig. 2, takes as input a complete monocular endoscopic video sequence, the corresponding binary occlusion masks, and depth maps. The

time component t_i of each frame i is normalized to $t_i = i/T$. We initialize our Surgical Gaussian Surfels from the PIMI (Sec. 3.2) reconstructed point cloud, representing each point as a surface-aligned elliptical splat characterized by a constrained covariance matrix, opacity value, and view-dependent color features represented by spherical harmonic coefficients. To model tissue deformation, we employ a lightweight MLP that predicts per-surfel motion fields while maintaining temporal consistency. The network is set to minimize the photometric differences between the input frames and the rendered views. We introduce several regularization terms to enforce surface smoothness and geometric consistency in occluded regions (Sec. 3.3). Our pipeline enables real-time rendering of dynamic surgical scenes while preserving fine surgical tissue details.

3.1 Preliminaries and Surgical Gaussian Surfels

3D Gaussian Splatting represents a scene as a set of anisotropic 3D Gaussian primitives $\{\mathcal{G}_k \mid k = 1, \dots, K\}$, each parameterized by its position $\mathbf{p}_k \in \mathbb{R}^3$, opacity $\alpha_k \in [0, 1]$, and scaling matrix $\mathbf{S}_k \in \mathbb{R}^{3 \times 3}$. The covariance matrix of \mathcal{G}_k in the world space is defined as $\boldsymbol{\Sigma}_k = \mathbf{O}_k \text{diag}(\mathbf{s}_k) \mathbf{O}_k^T$, where $\mathbf{s}_k \in \mathbb{R}^3$ is a scaling vector and $\mathbf{O}_k \in \mathbb{R}^{3 \times 3}$ is a rotation matrix parameterized by a quaternion. The Gaussian function is defined as $\mathcal{G}_k(\mathbf{x}) = e^{-\frac{1}{2}(\mathbf{x}-\mathbf{p}_k)^T \boldsymbol{\Sigma}_k^{-1}(\mathbf{x}-\mathbf{p}_k)}$. During rendering, Gaussians undergo a view transformation defined by rotation \mathbf{R} and translation \mathbf{t} , where $\mathbf{p}'_k = \mathbf{R}\mathbf{p}_k + \mathbf{t}$, $\boldsymbol{\Sigma}'_k = \mathbf{R}\boldsymbol{\Sigma}_k\mathbf{R}^T$ represent the view-space position and the covariance matrix, respectively. They are then projected to ray space through a local affine transformation $\boldsymbol{\Sigma}'_k^{2D} = \mathbf{J}_k \boldsymbol{\Sigma}'_k \mathbf{J}_k^T$, where \mathbf{J}_k approximates the projective transformation at the Gaussian center. The view-dependent appearance is modeled using spherical harmonics and alpha composition.

Our Surgical Gaussian Surfels adapt the 3D Gaussian Splatting approach by using surface-aligned elliptical splats, optimized for rendering deformable surgical scenes. Inspired by [6], each surfel ψ_k is parameterized by its position $\mathbf{p}_k \in \mathbb{R}^3$, two orthonormal tangential vectors $\mathbf{t}_u, \mathbf{t}_v \in \mathbb{R}^3$, and scaling factors $s_u, s_v \in \mathbb{R}$ that control the size of the Gaussian. The inherent primitive normal is shown in Fig. 2 as $\mathbf{n}_k = \mathbf{t}_u \times \mathbf{t}_v$ represents the direction of the steepest change in surfel density. This formulation enables direct gradient-based optimization, ensuring accurate surfel alignment with the surface of the surgical tissue.

The position of any point on the 2D Gaussian in world space is given by $P(u, v) = \mathbf{p}_k + s_u \mathbf{t}_u u + s_v \mathbf{t}_v v$, $u, v \in \mathbb{R}$, where (u, v) are local coordinates in the tangent plane. Using homogeneous coordinates, the transformation of the Gaussian from local to world space is represented as:

$$H = \begin{bmatrix} s_u t_u & s_v t_v & 0 & \mathbf{p}_k \\ 0 & 0 & 0 & 1 \end{bmatrix}, \quad (1)$$

where $H \in \mathbb{R}^{4 \times 4}$ encodes scaling, rotation, zeroed \mathbf{z} -component, and translation. As such, $\mathbf{R}_k \text{diag}(\mathbf{s}_k) = H_k[:, :3]$. It then follows that the density of each Surgical Gaussian Surfel primitive is modeled as:

$$\mathcal{G}_k(u, v) = \exp\left(-\frac{u^2 + v^2}{2}\right). \quad (2)$$

Gaussian surfel deformation and rasterization. We use a lightweight MLP to model the deformation field of Gaussian Surfel primitives [17]. The MLP accepts the high-frequency positional and time-encoded [12] surfel primitives corresponding to the current frame as input. The deformation model learns adjustments for various Gaussian properties, such as position, scaling, and rotation, to capture the motion within the scene. Similar to [6], our Surgical Gaussian Surfels are rasterized following a depth-sorted volumetric alpha blending approach:

$$c(x) = \sum_k c_k \alpha_k \hat{\mathcal{G}}_k(u(x)) \prod_{j=1}^{k-1} \left(1 - \alpha_j \hat{\mathcal{G}}_j(u(x))\right), \quad (3)$$

where c_k is the color of k -th Gaussian, α_k its opacity, and $\hat{\mathcal{G}}_k$ its adjusted Gaussian value. The process terminates once accumulated opacity reaches saturation.

3.2 PIMI Gaussian Surfel Primitive Initialization

Xie et al. [17] initialize a surgical scene point cloud by projecting visible pixels from depth maps and binary masks into 3D space. However, when depth data are incomplete, this results in noticeable gaps in the reconstructed point cloud and inaccuracies in the initialization due to color and geometric incongruencies.

To mitigate these issues, we propose an initialization method, termed *Projection-Based Iterative Mask Integration (PIMI)*, which improves the quality and completeness of the initial point cloud by leveraging confidence-weighted depth aggregation and aggregated color mapping. The depth map D_t for each frame is pre-processed to create a confidence-weighted depth map D^* using a thresholded confidence mask, which ensures the exclusion of noisy depth data. Simultaneously, we aggregate the color maps C_t to compute the refined color map C^* . This aggregation scheme at timestep t is defined as:

$$D^* = \frac{\sum_{t=1}^T D_t \cdot W_t}{\sum_{t=1}^T W_t}, \quad C^* = \frac{\sum_{t=1}^T C_t \cdot W_t}{\sum_{t=1}^T W_t} \quad (4)$$

where W_t is the confidence mask derived by identifying reliable depth values within the 2nd to 99th percentile range of the depth distribution. Using D^* and C^* , we generate the refined point cloud P^* . Each 2D pixel coordinate (x, y) is projected into 3D space based on the intrinsic camera parameters K as:

$$p(x, y) = D^*(x, y) \cdot K^{-1} \begin{bmatrix} x \\ y \\ 1 \end{bmatrix}, \quad P^* = \{(p_i, C_i^*)\}_{i=1}^N, \quad (5)$$

where P^* is the final point cloud, with p_i as the 3D points and C_i^* as their RGB colors encoded via spherical harmonics coefficients. This sequential integration of depth and color ensures geometric consistency and accurate color representation of the projected surgical scene.

3.3 Optimization

To capture fine details of surgical tissue and render areas occluded by surgical tools, we invert the binary mask in occluded areas and employ a weighted total loss consisting of photometric loss [14], total variation (TV) loss [11], deformation regularization, VGG16 [15] perceptual loss, and normal consistency:

$$L = \lambda_1 L_{\text{photo}} + \lambda_2 L_{\text{tv}} + \lambda_3 L_{\text{pos}} + \lambda_4 L_{\text{cov}} + \lambda_5 L_{\text{per}} + \lambda_6 L_{\text{n}}. \quad (6)$$

Deformation regularization. In single-view surgical video, surfel motion can become unstable without constraints. To ensure coherent yet flexible deformation, we use a deformation regularization that maintains relative distances between neighboring surfels before and after deformation. Given a surfel ψ_k , we enforce consistency across its K nearest neighbors (where $K = 5$) [17] in both position and scaling:

$$L_{\text{pos}} = \sum_k \sum_{j \in \mathcal{N}(k)} \left\| d(\mathbf{x}^{(k)}, \mathbf{x}^{(j)}) - d(\hat{\mathbf{x}}^{(k)}, \hat{\mathbf{x}}^{(j)}) \right\|_1, \quad (7)$$

$$L_{\text{cov}} = \sum_k \sum_{j \in \mathcal{N}(k)} \left\| d(\mathbf{s}^{(k)}, \mathbf{s}^{(j)}) - d(\hat{\mathbf{s}}^{(k)}, \hat{\mathbf{s}}^{(j)}) \right\|_1. \quad (8)$$

where $d(\cdot, \cdot)$ computes the Euclidean distance, and $\mathbf{x}, \hat{\mathbf{x}}$ and $\mathbf{s}, \hat{\mathbf{s}}$ denote initial and deformed surfel positions and scaling factors, respectively.

Normal consistency. The normal consistency term enforces alignment between the rendered normals and the implicit normals derived from the geometric properties of the scene. This regularization ensures that all Gaussian surfels are locally aligned with the tissue surfaces. The loss is defined as:

$$L_{\text{n}} = \alpha \cdot (1 - \cos(\mathbf{n}_{\text{rendered}}, \mathbf{n}_{\text{expected}})) + \beta \cdot (1 - \cos(\mathbf{n}_{\text{rendered}}, \mathbf{n}_{\text{median}})), \quad (9)$$

where $\mathbf{n}_{\text{rendered}}$, $\mathbf{n}_{\text{expected}}$, and $\mathbf{n}_{\text{median}}$ are the rendered normals, the expected normals from surface geometry (i.e., gradient of the depth map), and the normals of surfels at the median intersection point along the viewing ray, respectively. The weights α and β balance the contributions of the two alignment targets.

4 Experiments

Datasets and evaluation. We evaluate our method on two publicly available datasets, EndoNeRF [16] and StereoMIS [5]. The EndoNeRF dataset captures two cases of an in-vivo DaVinci robot prostatectomy from a single viewpoint. We evaluate on four video sequences of the StereoMIS dataset, which shows porcine subject breathing and tissue deformation during a liver and intestinal procedure. We estimate scene depth on the StereoMIS dataset using a pre-trained Omnidata [3] model and tool occlusion binary masks using a pre-trained SAM2 [13] model. We measure the surgical scene reconstruction capabilities of SGS using

Table 1: Quantitative comparisons of our method SGS with EndoNeRF [16], EndoSurf [20], LerPlane [18], EndoGaussian [10], and SurgicalGaussian (SG) [17].

Dataset	Methods	"pulling"			"cutting"			Rendering	
		LPIPS↓	PSNR↑	SSIM↑	LPIPS↓	PSNR↑	SSIM↑	FPS↑	GPU↓
EndoNeRF	EndoNeRF	0.080	29.088	0.930	0.106	26.792	0.901	0.04	15 GB
	EndoSurf	0.111	36.919	0.961	0.103	35.551	0.955	0.05	17 GB
	LerPlane	0.085	36.272	0.936	0.114	33.774	0.901	1.02	20 GB
	EndoGaussian	0.089	36.429	0.951	0.102	35.773	0.956	190	2 GB
	SG	0.049	38.783	0.970	0.062	37.505	0.961	80	4 GB
	Ours	0.027	39.059	0.971	0.027	37.609	0.965	66	2 GB
StereoMIS		"intestine"			"liver"			FPS↑	GPU↓
		0.153	30.510	0.833	0.316	27.370	0.680	0.06	13 GB
		0.204	29.660	0.853	0.248	28.941	0.820	0.08	14 GB
		0.206	29.441	0.822	0.254	28.852	0.793	1.45	19 GB
		0.213	29.024	0.805	0.295	26.174	0.728	200	2 GB
		0.145	31.496	0.890	0.135	31.668	0.893	140	3 GB
	Ours	0.048	34.669	0.936	0.047	34.390	0.934	81	2 GB

Table 2: Ablation study on EndoNeRF [16] dataset.

Model	"pulling"			"cutting"		
	LPIPS↓	PSNR↑	SSIM↑	LPIPS↓	PSNR↑	SSIM↑
w/o Perceptual loss	0.028	38.911	0.970	0.032	37.307	0.962
w/o Photometric loss	0.028	38.852	0.970	0.043	35.566	0.957
w GIDM initialization	0.027	38.907	0.970	0.031	37.380	0.963
Full model (PIMI init)	0.027	39.059	0.971	0.027	37.609	0.965

three standard metrics: LPIPS, PSNR, and SSIM. Our method achieves state-of-the-art (SOTA) results on all metrics.

Implementation details. All experiments are carried out on an NVIDIA RTX A6000, using the PyTorch framework. Adam [9] optimizer is used during training. The loss weights in Eq. (6) were set empirically to: $\lambda_1 = 0.7$, $\lambda_2 = 0.006$, $\lambda_3 = 1.0$, $\lambda_4 = 200.0$, $\lambda_5 = 1.0$, $\lambda_6 = 0.0001$.

4.1 Main Results and Ablation

We compare SGS against existing methods for real-time rendering of surgical scenes in the EndoNeRF [16] and StereoMIS [5] datasets. SDF-based approaches such as EndoSurf [20] require separate MLPs for deformation, geometry, and appearance, which increases computational complexity and limits real-time performance. Neural LerPlane [18] factorizes 4D scenes into 2D planes to reduce overhead, but struggles to capture complex deformations. EndoGaussian [10] shifts towards explicit depth-aware point clouds but relies heavily on pre-initialized geometry, making it less adaptable to dynamic changes. Lastly, SurgicalGaussian [17] introduces a deformation network that decouples motion and geometry,

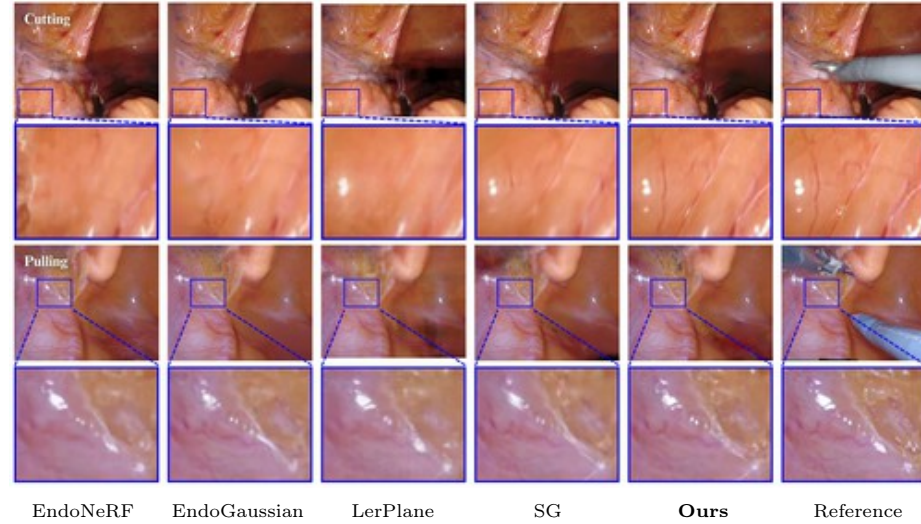


Fig. 3: Qualitative comparisons of our method (SGS) with EndoNeRF [16], EndoSurf [20], LerPlane [18], EndoGaussian [10], and SG [17].

but struggles to render fine details in the surgical scene. SGS outperforms these previous methods in all datasets, achieving the lowest LPIPS, the highest PSNR and the highest SSIM, while qualitatively capturing specularity and anatomical features more accurately, as shown in Tab. 1 and Fig. 3.

Ablation study. We perform ablation studies in a "leave-one-out" fashion on the EndoNeRF [20] dataset. To assess the impact of our PIMI Gaussian initialization, we replace it with the prior SOTA GIDM [17] point cloud initialization. We also provide test-time results without perceptual, photometric, and TV loss. The results are summarized in Tab. 2. Homodirectional view-space positional gradients [19] are used during Gaussian Surfel densification for all experiments.

5 Conclusion

In this article, we introduce Surgical Gaussian Surfels (SGS), an explicit rendering method that takes advantage of the accurate geometry reconstruction capabilities of surface-aligned anisotropic splats. We utilize scale-constrained elliptical primitives to produce high-fidelity renders of surgical scenes. We define surface normals as the direction of the steepest density change, thereby generating accurate surgical tissue surface normals without normal priors. By leveraging both Projection-Based Iterative Mask Integration (PIMI) for robust point-cloud initialization and Gaussian Surfel densification based on homodirectional view-space positional gradients, our method achieves state-of-the-art reconstruction quality with real-time rendering performance. SGS has the potential to advance

surgical scene understanding and support a range of intraoperative applications, including surgical navigation and robot-aided surgical procedures.

References

- Dai, P., Xu, J., Xie, W., Liu, X., Wang, H., Xu, W.: High-quality surface reconstruction using gaussian surfels. In: ACM SIGGRAPH 2024 Conference Papers. pp. 1–11 (2024) 2
- Dupont, P.E., Nelson, B.J., Goldfarb, M., Hannaford, B., Menciassi, A., O’Malley, M.K., Simaan, N., Valdastri, P., Yang, G.Z.: A decade retrospective of medical robotics research from 2010 to 2020. *Science Robotics* **6**(60) (2021) 1
- Eftekhari, A., Sax, A., Malik, J., Zamir, A.: Omnidata: A scalable pipeline for making multi-task mid-level vision datasets from 3d scans. In: Proceedings of the IEEE/CVF International Conference on Computer Vision. pp. 10786–10796 (2021) 6
- Haidegger, T.: Autonomy for surgical robots: Concepts and paradigms. *IEEE Transactions on Medical Robotics and Bionics* **1**(2), 65–76 (2019) 2
- Hayoz, M., Max, A.: Stereomis. Zenodo (2023). <https://doi.org/10.5281/zenodo.7727692> 2, 6, 7
- Huang, B., Yu, Z., Chen, A., Geiger, A., Gao, S.: 2d gaussian splatting for geometrically accurate radiance fields. In: ACM SIGGRAPH 2024 Conference Papers. pp. 1–11 (2024) 4, 5
- Huang, Y., Cui, B., Bai, L., Guo, Z., Xu, M., Ren, H.: Endo-4dgs: Distilling depth ranking for endoscopic monocular scene reconstruction with 4d gaussian splatting. arXiv preprint arXiv:2401.16416 (2024) 3
- Kerbl, B., Kopanas, G., Leimkühler, T., Drettakis, G.: 3d gaussian splatting for real-time radiance field rendering. *ACM Transactions on Graphics* **42**(4), 139–1 (2023) 2
- Kingma, D., Ba, J.: Adam: A method for stochastic optimization. arXiv preprint arXiv:1412.6980 (2014) 7
- Liu, Y., Li, C., Yang, C., Yuan, Y.: Endogaussian: Gaussian splatting for deformable surgical scene reconstruction. arXiv preprint arXiv:2401.12561 (2024) 3, 7, 8
- Mahendran, A., Vedaldi, A.: Understanding deep image representations by inverting them. In: Proceedings of the IEEE Conference on Computer Vision and Pattern Recognition (2015) 6
- Mildenhall, B., Srinivasan, P.P., Tancik, M., Barron, J.T., Ramamoorthi, R., Ng, R.: NeRF: Representing scenes as neural radiance fields for view synthesis. *Communications of the ACM* **65**(1), 99–106 (2021) 5
- Ravi, N., Gabeur, V., Hu, Y.T., Hu, R., Ryali, C., Ma, T., Khedr, H.e.a.: SAM 2: Segment anything in images and videos. arXiv preprint arXiv:2408.00714 (2024) 6
- Shen, T., Luo, Z., Zhou, L., Deng, H., Zhang, R., Fang, T., Quan, L.: Beyond photometric loss for self-supervised ego-motion estimation. In: 2019 International Conference on Robotics and Automation (ICRA). pp. 6359–6365. IEEE (2019) 6
- Simonyan, K., Zisserman, A.: Very deep convolutional networks for large-scale image recognition. arXiv preprint arXiv:1409.1556 (2014) 6
- Wang, Y., Long, Y., Fan, S.H., Dou, Q.: Neural rendering for stereo 3d reconstruction of deformable tissues in robotic surgery. In: International Conference on Medical Image Computing and Computer-Assisted Intervention. pp. 431–441. Springer Nature Switzerland, Cham (2022) 3, 6, 7, 8
- Xie, W., Yao, J., Cao, X., Lin, Q., Tang, Z., Dong, X., Guo, X.: Surgicalgaussian: Deformable 3d gaussians for high-fidelity surgical scene reconstruction. In: International Conference on Medical Image Computing and Computer-Assisted Intervention. pp. 617–627. Springer Nature Switzerland, Cham (2024) 3, 5, 6, 7, 8

18. Yang, C., Wang, K., Wang, Y., Yang, X., Shen, W.: Neural lerplane representations for fast 4d reconstruction of deformable tissues. In: International Conference on Medical Image Computing and Computer-Assisted Intervention. pp. 46–56. Springer Nature Switzerland, Cham (2023) [3](#), [7](#), [8](#)
19. Ye, Z., Li, W., Liu, S., Qiao, P., Dou, Y.: Absgs: Recovering fine details in 3d gaussian splatting. In: Proceedings of the 32nd ACM International Conference on Multimedia. pp. 1053–1061 (2024) [8](#)
20. Zha, R., Cheng, X., Li, H., Harandi, M., Ge, Z.: Endosurf: Neural surface reconstruction of deformable tissues with stereo endoscope videos. In: International Conference on Medical Image Computing and Computer-Assisted Intervention. pp. 13–23. Springer Nature Switzerland, Cham (2023) [3](#), [7](#), [8](#)